Supporting Information

Amplifiable Symmetry Breaking in Aggregates of Vibrating Helical Molecules

Fang Wang, Fuwei Gan, Chengshuo Shen, and Huibin Qiu*

School of Chemistry and Chemical Engineering, Frontiers Science Center for Transformative Molecules, State Key Laboratory of Metal Matrix Composites, Shanghai Jiao Tong University, Shanghai 200240, China.

E-mail: hbqiu@sjtu.edu.cn (H. Qiu).

1 Experimental section

1.1 Instruments and methods

CD spectra of suspension and solution samples were measured in quartz cuvettes (light path length 10 mm) on a JASCO J-815 CD spectrometer. Temperature interval experiments were carried out with a temperature gradient of 2 °C/min and waiting time of 60 s in the heating process. For the CD spectra of freeze-dried aggregates, the samples were first mixed with KBr and casted into plates, and then the plates were placed perpendicular to the light path of CD spectrometer and rotated within the plate plane to rule out the possibility of birefringency and eliminate the possible angle dependence of the CD signal.

Circularly polarized luminescence (CPL) spectra were recorded in quartz cuvettes with an optical path length of 10 mm using a JASCO CPL-300 spectrometer.

UV-visible (UV-vis) absorption spectra were recorded using Shimadzu UV-2600 Spectrometer at 20 °C in a 1 mm quartz cell.

The fluorescence spectra were recorded on a LS 55 from Perkin Elmer, Inc., USA.

SEM was performed on a JEOL JSM-7800F microscope with an accelerating voltage of 5 kV. Samples were prepared by dropping ca. 50–100 μL of suspension onto a polished silicon wafer, followed by drying and coating with a thin layer of Au to enhance the contrast.

Transmission electron microscopy (TEM) was performed on a JEM-1400 plus microscope at an accelerating voltage of 120 kV. The TEM samples were prepared by casting a small amount of sample onto a copper omentum and dried overnight in the air.

Single crystal X-ray diffraction measurements were performed on a Bruker SMART Apex II CCD-based X-ray diffractometer with Mo-Kαradiation (λ = 0.71073 Å). Powder X-ray diffraction (PXRD) data were collected on a D8 Advance instrument from Bruker-AXS Company over 2θ range of 3.0°–30.0° at room temperature. Freeze-dried samples were cast on glass substrates for PXRD measurements.

1.2 Materials

All starting materials and solvents were of AR grade quality, which were purchased from commercial sources and used without any further purification. 2-Aza[4]helicene, 4-aza[4]helicene, and naphtho[2,1-f]quinoline were synthesized according to a previous report and NMR data was in well agreement with the literature.[S1]

2 Additional experimental data and figures

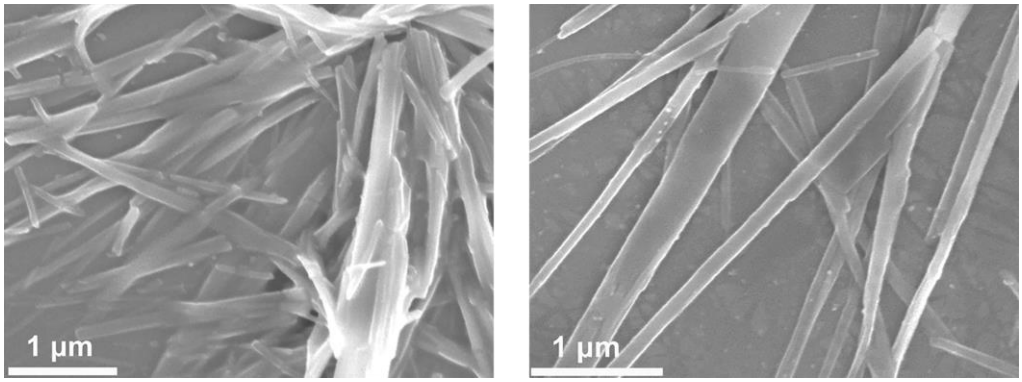

Figure S1. Additional SEM images of dried 2-A[4]H aggregates obtained in DMF/H_2O (1/99, v/v) with a concentration of 1.3×10^{-3} mol·L^{-1}.

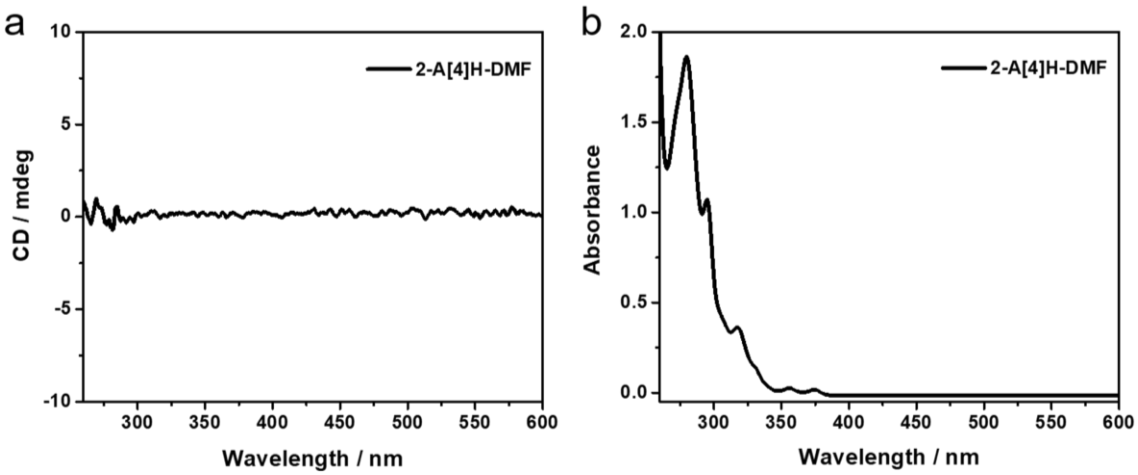

Figure S2. (a) CD and (b) UV–vis spectra of 2-A[4]H in DMF with a concentration of 0.22×10^{-3} mol·L^{-1}.

Racemization barriers of 2-A[4]H and 4-A[4]H

Density functional theory (DFT) calculations were carried out using Gaussian 09 program. Geometrical optimization calculations were carried out at the PBE0-D3(BJ)/def2-SVP level without any symmetry assumptions unless otherwise stated. Harmonic vibration frequency calculations were performed at the same level for verifying the resulting geometries as local minima (with all the frequencies real) or saddle points (with only one imaginary frequency). The assignment of the saddle points was performed using intrinsic reaction coordinate (IRC) calculations.

Table S1. Calculated enthalpies $\Delta H^{\ddagger}_{calc}$ and free energies $\Delta G^{\ddagger}_{calc}$ (in kcal·mol^{-1} at 298.15 K)

	$\Delta H^{\ddagger}_{calc}$	$\Delta G^{\ddagger}_{calc}$
2-A[4]H	3.58	4.25
4-A[4]H	3.48	4.15

Cartesian coordinates of the optimized geometries

2-A[4]H

C	0.021488	1.812785	0.002846	C	−3.721636	−0.156259	−0.178136	H	−1.135146	3.636007	−0.216368
C	0.009298	0.398565	0.002990	C	−3.834514	−1.500408	0.099380	H	−3.301991	2.467017	−0.498388
C	1.288147	−0.278508	−0.049836	C	−2.681913	−2.233348	0.434351	H	−4.612038	0.443861	−0.382506
C	2.487419	0.457126	0.177982	C	−1.439574	−1.633140	0.416828	H	−4.813517	−1.984817	0.099082
C	2.433239	1.873094	0.333319	C	1.464814	−1.633360	−0.442906	H	−2.768445	−3.281483	0.729650
C	1.246850	2.523917	0.186051	N	2.618419	−2.263658	−0.471413	H	−0.577115	−2.214019	0.737959
C	−1.189985	2.545360	−0.176388	C	3.723962	−1.588134	−0.113372	H	0.606205	−2.201130	−0.809727
C	−2.382068	1.904578	−0.321267	C	3.713154	−0.242560	0.178681	H	4.660797	−2.155690	−0.107230
C	−2.463353	0.488991	−0.170825	H	3.359999	2.422411	0.514138	H	4.643159	0.293818	0.381558
C	−1.274669	−0.271308	0.057403	H	1.205211	3.615298	0.229112				

2-A[4]H (racemization transition state)

C	0.019584	1.757825	0.000140	C	−3.781678	−0.068528	−0.000343	H	−1.094619	3.614718	0.000126
C	0.008749	0.335611	0.000096	C	−3.963795	−1.430376	−0.000193	H	−3.317355	2.515091	−0.000330
C	1.322029	−0.318847	0.000027	C	−2.826556	−2.251002	0.000293	H	−4.641452	0.606198	−0.000599
C	2.511716	0.479625	−0.000030	C	−1.557791	−1.708134	0.000392	H	−4.966437	−1.863110	−0.000373
C	2.444258	1.899803	0.000130	C	1.581775	−1.720905	0.000018	H	−2.934774	−3.338026	0.000628
C	1.233980	2.507859	0.000236	N	2.767727	−2.291261	−0.000110	H	−0.749093	−2.422434	0.000871
C	−1.181463	2.525850	0.000052	C	3.860399	−1.515222	−0.000259	H	0.773144	−2.440936	0.000120
C	−2.396866	1.926821	−0.000189	C	3.777117	−0.144699	−0.000192	H	4.828587	−2.027264	−0.000405
C	−2.489734	0.508282	−0.000169	H	3.372478	2.475288	0.000155	H	4.677307	0.474423	−0.000249
C	−1.308526	−0.309456	0.000082	H	1.158936	3.597839	0.000293				

4-A[4]H

C	0.025617	1.803068	0.006355	C	2.437388	1.850474	0.321159	C	−2.467258	0.490979	−0.173044
C	0.005535	0.389262	0.005079	C	1.255355	2.509169	0.180321	C	−1.282246	−0.274195	0.056752
C	1.279254	−0.298304	−0.053102	C	−1.183441	2.540696	−0.170865	C	−3.728386	−0.148593	−0.184208
C	2.486879	0.432447	0.174615	C	−2.378593	1.906630	−0.319458	C	−3.849163	−1.492451	0.092007

C	−2.700915	−2.229803	0.431568	H	3.382965	2.367749	0.490550	H −2.793688 −3.276626 0.730060
C	−1.455763	−1.634707	0.417308	H	1.220216	3.600870	0.219454	H −0.598202 −2.217163 0.748696
C	1.449908	−1.649731	−0.439299	H	−1.123059	3.631095	−0.209345	H 0.596489 −2.232885 −0.781786
C	2.705469	−2.217716	−0.445579	H	−3.295264	2.474289	−0.496989	H 2.850417 −3.254687 −0.755226
C	3.806878	−1.426203	−0.069636	H	−4.615373	0.456146	−0.390050	H 4.811374 −1.864807 −0.026943
N	3.707926	−0.145429	0.200410	H	−4.830467	−1.972119	0.088869	

4-A[4]H (racemization transition state)

C	0.023764	1.751052	−0.000032	C	−3.785504	−0.063237	−0.000187	H −1.085024 3.610600 0.000064
C	0.006349	0.329236	0.000176	C	−3.973465	−1.424434	−0.000097	H −3.311406 2.518933 −0.000322
C	1.313525	−0.334161	−0.000022	C	−2.839215	−2.248758	0.000318	H −4.642648 0.614877 −0.000342
C	2.513937	0.458373	0.000237	C	−1.568348	−1.709993	0.000616	H −4.977698 −1.853381 −0.000193
C	2.447596	1.879474	0.000034	C	1.564328	−1.730801	−0.000695	H −2.951721 −3.335434 0.000503
C	1.241533	2.495309	−0.000264	C	2.844608	−2.240306	−0.000607	H −0.764656 −2.429451 0.001317
C	−1.175510	2.522034	0.000009	C	3.929442	−1.351943	0.000234	H 0.765260 −2.456868 −0.001895
C	−2.393035	1.927300	−0.000116	N	3.765706	−0.051978	0.000508	H 3.008226 −3.319851 −0.001158
C	−2.491600	0.508863	−0.000138	H	3.394231	2.421062	0.000165	H 4.960406 −1.726270 0.000524
C	−1.312962	−0.312345	0.000226	H	1.172432	3.585657	−0.000374	

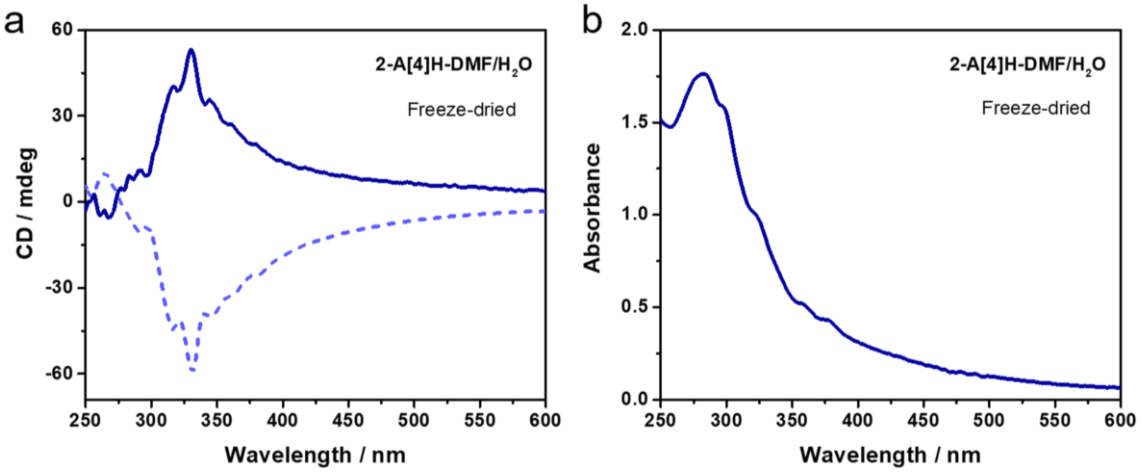

Figure S3. (a) CD and (b) UV–vis spectra of freeze-dried 2-A[4]H aggregates formed in DMF/H_2O (1/99, v/v) with a concentration of 1.3×10^{-3} mol·L^{-1}.

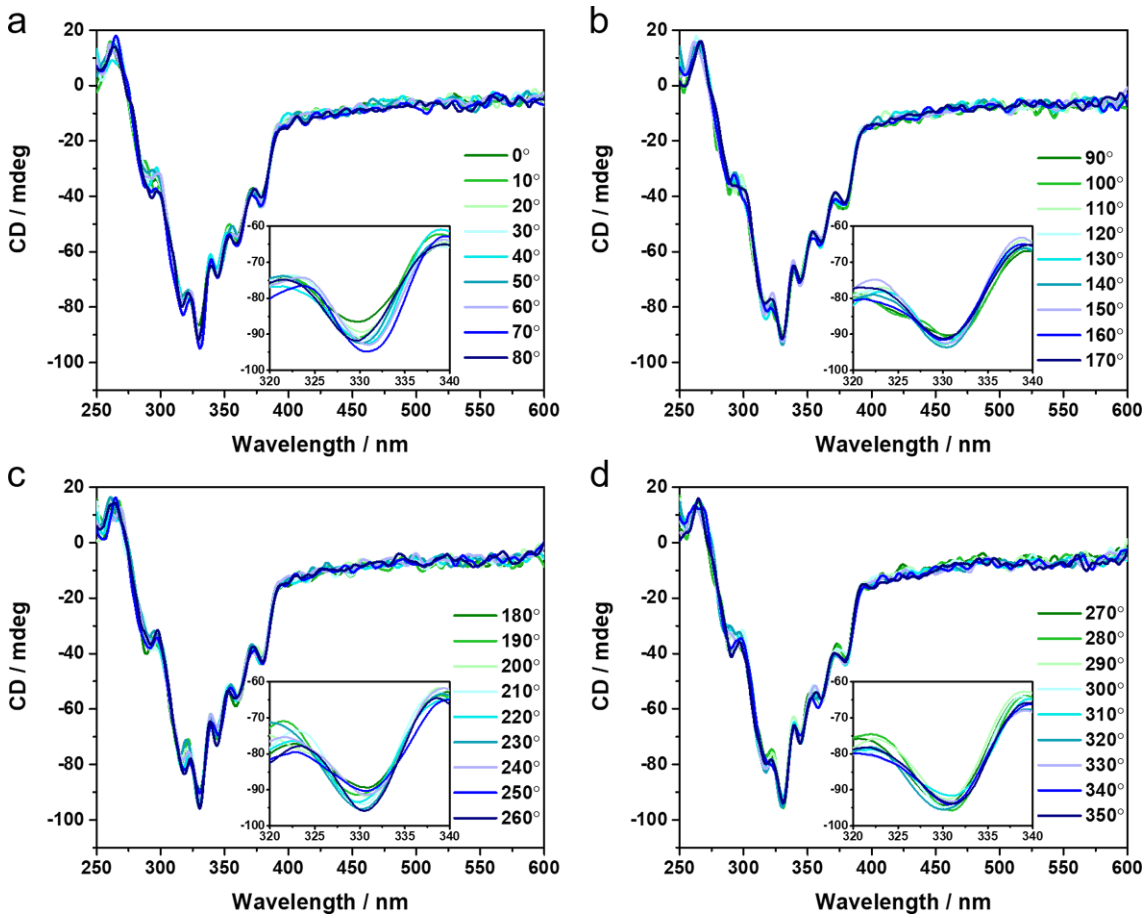

Figure S4. CD spectra of a plate formed by 2-A[4]H aggregates and KBr at different rotating angles in the range of (a) 0°~80°, (b) 90°~170°, (c) 180°~260°, (d) 270°~350°, with an interval of 10°. The 36 individual CD spectra showed slightly different CD amplitude, indicating a weak LD effect.

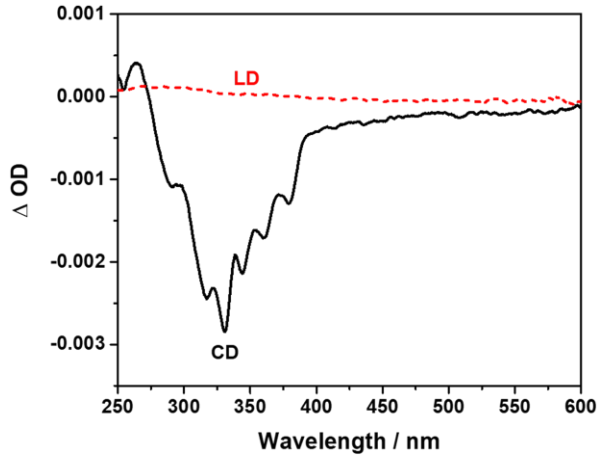

Figure S5. Mean spectrum of all 36 CD spectra (in ΔOD, solid black line) for comparison with mean spectrum of all 36 LD spectra (dash red line). To investigate the contribution of LD on the CD signals, the film of 2-A[4]H aggregate was placed in different angles and average CD and LD signals were taken according to reported procedures in literature.[S2] Compared to the mean spectrum of all 36 CD spectra, the mean spectrum of all 36 LD spectra was in much low intensity and thus the contribution was negligible.

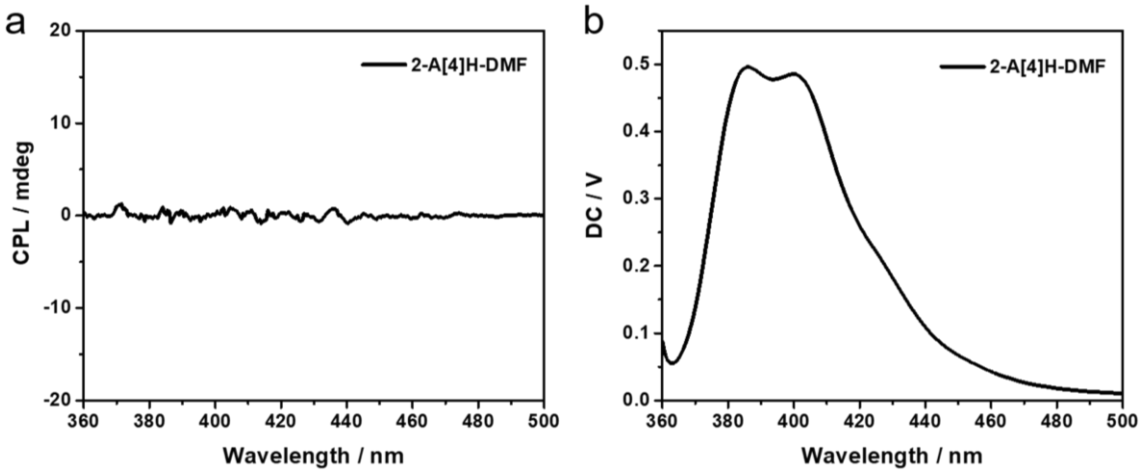

Figure S6. (a) CPL and (b) fluorescence spectra of 2-A[4]H in DMF with a concentration of 0.22 × 10^{-3} mol·L^{-1}.

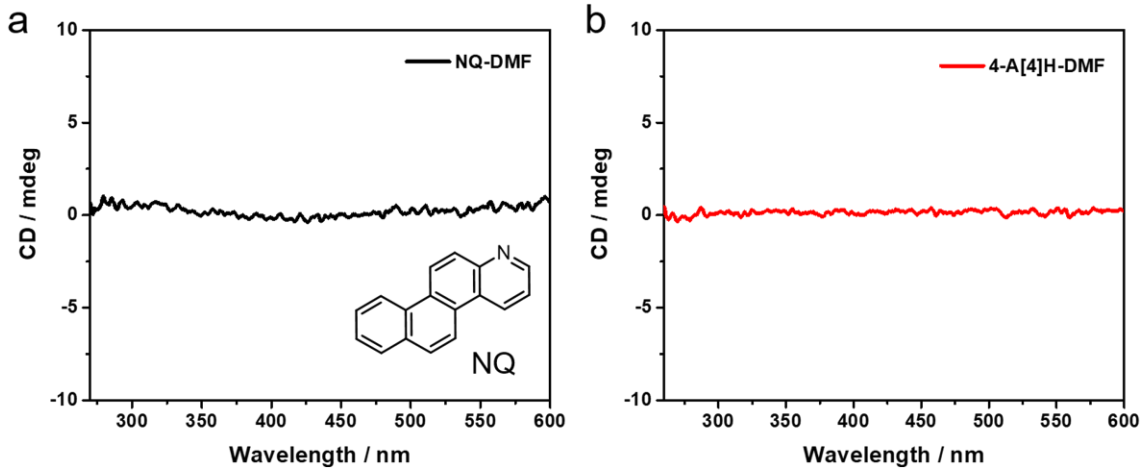

Figure S7. CD spectra of (a) NQ and (b) 4-A[4]H in DMF with a concentration of 0.22 × 10^{-3} mol·L^{-1}.

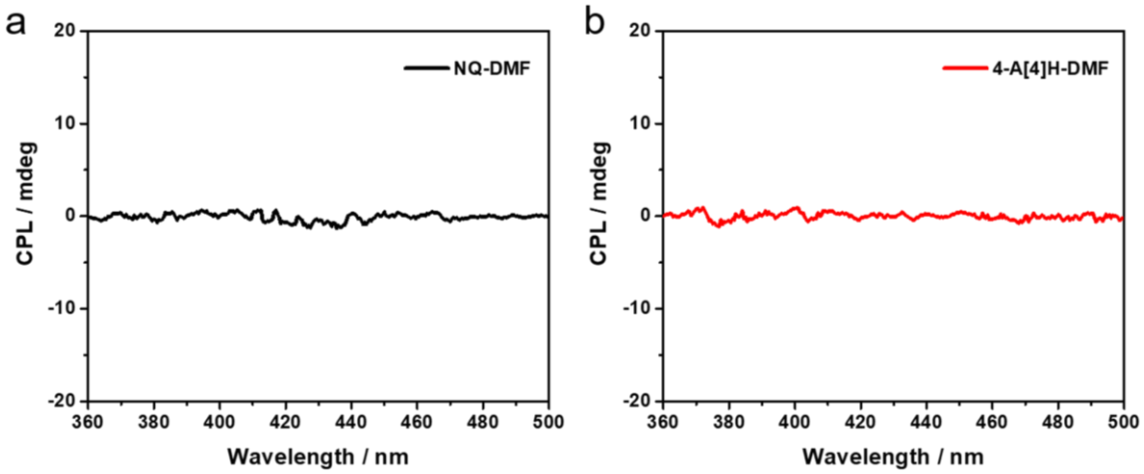

Figure S8. CPL spectra of (a) NQ and (b) 4-A[4]H in DMF with a concentration of 0.22 × 10^{-3} mol·L^{-1}.

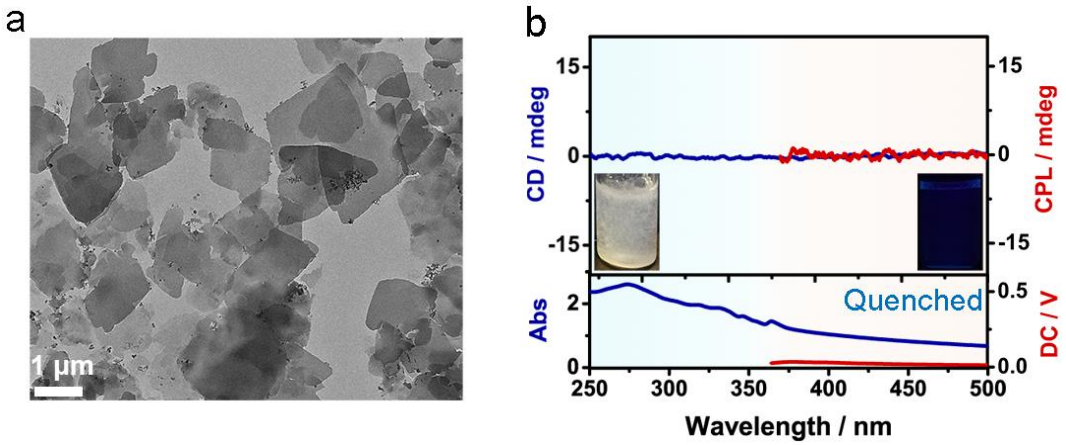

Figure S9. (a) TEM image of NQ aggregates formed in DMF/H_2O (1/99, v/v). (b) UV–vis, CD, fluorescence, and CPL spectra of NQ aggregates. The insets are the photographs of NQ aggregates before and after UV irradiation.

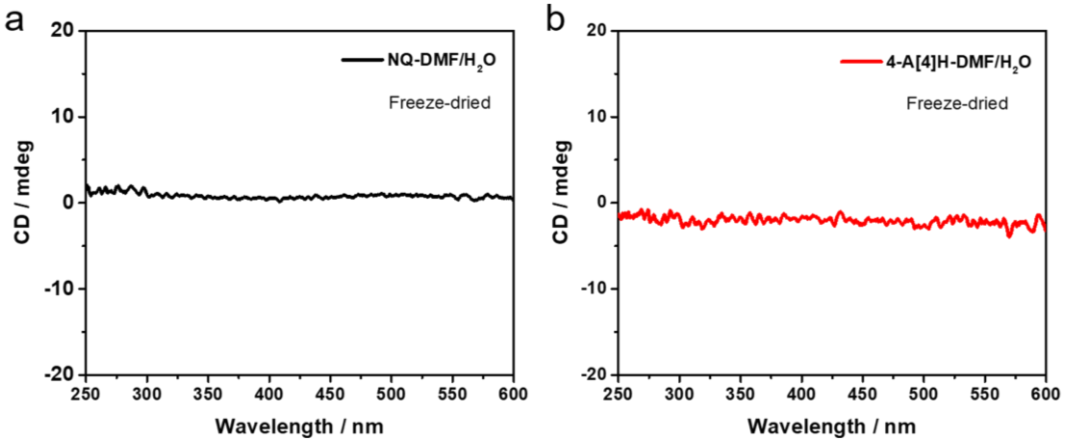

Figure S10. CD spectra of freeze-dried (a) NQ aggregates and (b) 4-A[4]H crystals formed in DMF/H_2O (1/99, v/v) with a concentration of 1.3×10^{-3} mol·L^{-1}.

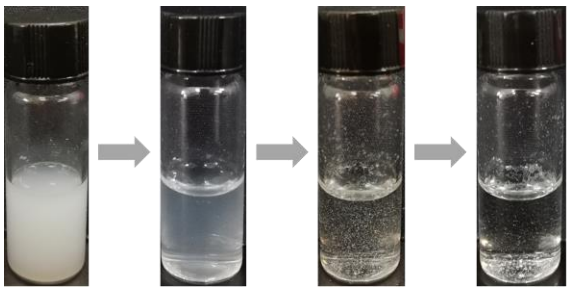

Figure S11. Photographs of 2-A[4]H aggregates formed at different time periods. After the addition of water into a DMF solution 2-A[4]H initially formed a white turbid dispersion and gradually transformed into a suspension containing visible small-size aggregates.

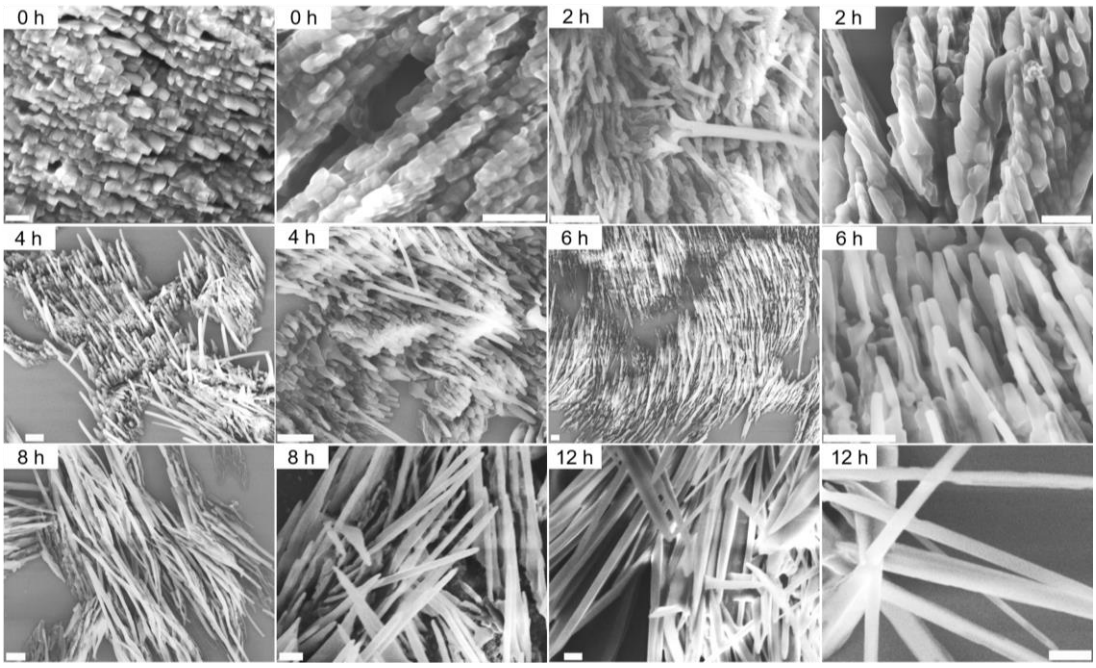

Figure S12. Additional SEM images of various aggregates formed by 2-A[4]H in DMF/H_2O (1/99, v/v) at different time periods. Scale bar = 1 μm. The concentration of 2-A[4]H is 1.3×10^{-3} mol·L^{-1}.

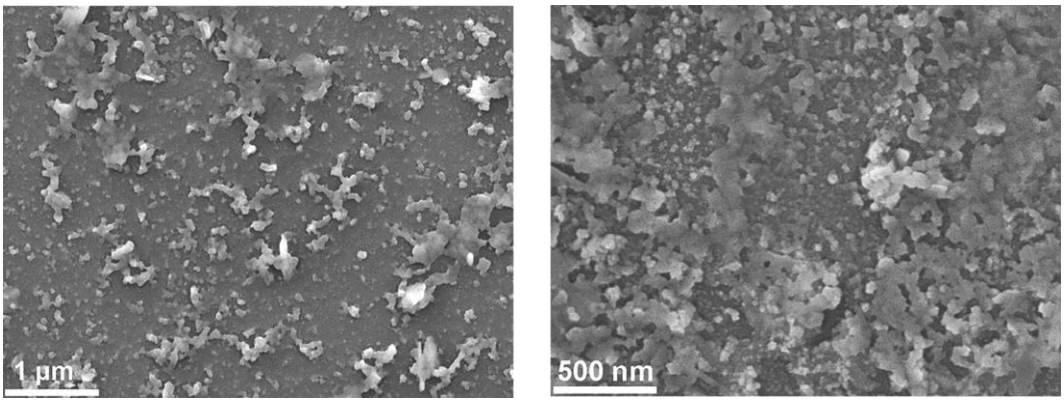

Figure S13. SEM images of dried 2-A[4]H aggregates obtained in DMF/H_2O (1/99, v/v) around 70 °C with a concentration of 1.3×10^{-3} mol·L^{-1}.

Table S2. Crystal data and structure refinement for a single crystal of **2-A[4]H** formed in acetone/*n*-pentane

Identification code	2-A[4]H
Empirical formula	$C_{17}H_{11}N$
Formula weight	229.283
Temperature/K	173.0
Crystal system	monoclinic
Space group	$P2_1$
a/Å	5.6278(4)
b/Å	14.1579(11)
c/Å	7.4484(6)
α/°	90
β/°	105.406(5)
γ/°	90
Volume/Å^3	572.15(8)
Z	2
$\rho_{Calculated}$/g·cm^{-3}	1.331
μ/mm^{-1}	0.597
F(000)	240.7
Crystal size/mm^3	0.1 × 0.1 × 0.1
Radiation	CuKα (λ = 1.54178)
2θ range for data collection/°	12.32 to 130.32
Index ranges	-6 ≤ h ≤ 6, -16 ≤ k ≤ 16, -8 ≤ l ≤ 8
Reflections collected	6158
Independent reflections	1950 [R_{int} = 0.0560, R_{sigma} = 0.0573]
Data/restraints/parameters	1950/1/163
Goodness-of-fit on F^2	1.067
Final R indexes [I>=2σ (I)]	R_1 = 0.0585, wR_2 = 0.1476
Final R indexes [all data]	R_1 = 0.0658, wR_2 = 0.1559
Largest diff. peak/hole / e Å^{-3}	0.33/-0.22
Flack parameter	-0.7(12)

It should be noted that due to the limited quality of the obtained crystals, the high angle data was dominated by noise. As a concequnce, one “Alert level A” occured after the checkCIF procedure.

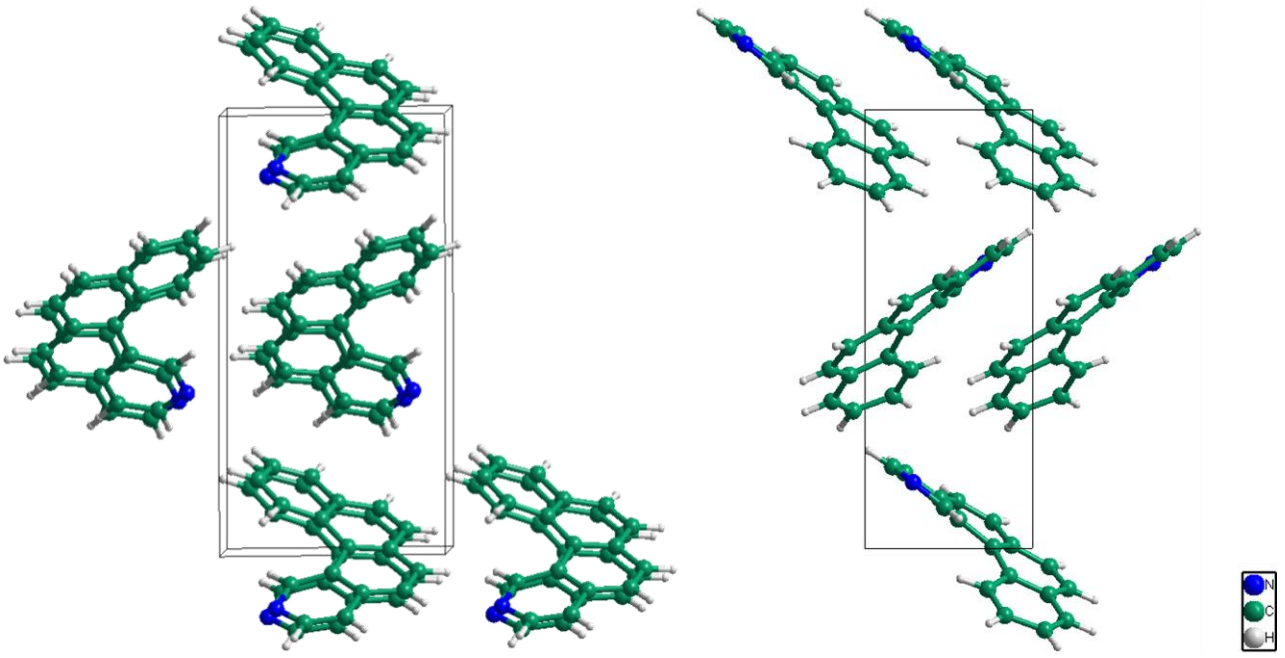

Figure S14. Single-crystal structure of 2-A[4]H obtained from an acetone/*n*-pentane mixture by gaseous phase diffusion.

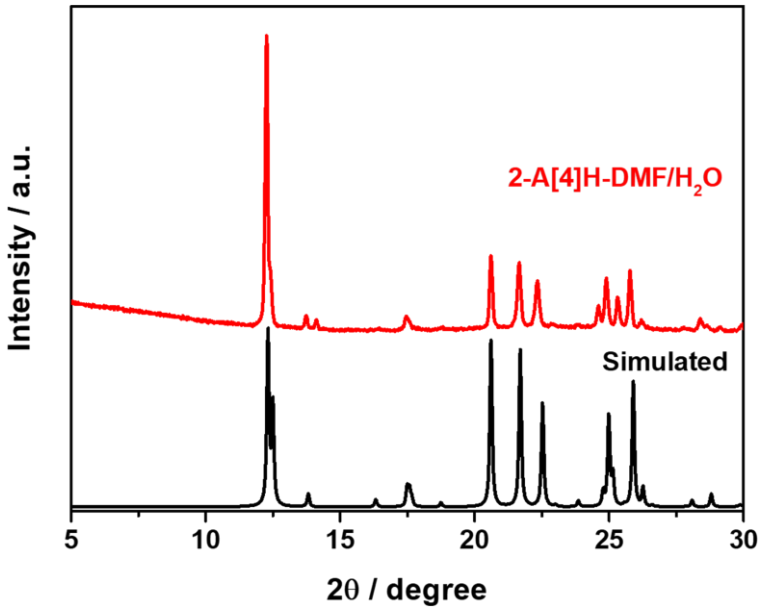

Figure S15. Comparison between simulated powder XRD pattern of a 2-A[4]H crystal formed in a acetone/*n*-pentane mixture and measured powder XRD pattern of 2-A[4]H aggregates prepared in DMF/H_2O (1/99, v/v).

Table S3. Crystal data and structure refinement for a single crystal of **4-A[4]H** formed in DMF/H_2O

Identification code	4-A[4]H
Empirical formula	$C_{17}H_{11}N$
Formula weight	229.283
Temperature/K	191.65
Crystal system	orthorhombic
Space group	*P*na2_1
a/Å	9.7299(19)
b/Å	22.520(5)
c/Å	5.2706(11)
α/°	90
β/°	90
γ/°	90
Volume/Å^3	1154.9(4)
Z	4
$\rho_{Calculated}$ /g·cm^{-3}	1.319
μ/mm^{-1}	0.592
F(000)	481.4
Crystal size/mm^3	0.12 × 0.1 × 0.08
Radiation	CuKα (λ = 1.54178)
2*θ* range for data collection/°	7.86 to 127.3
Index ranges	-11 ≤ h ≤ 9, -25 ≤ k ≤ 26, -5 ≤ l ≤ 5
Reflections collected	5796
Independent reflections	1747 [R_{int} = 0.0605, R_{sigma} = 0.0614]
Data/restraints/parameters	1747/2/163
Goodness-of-fit on F^2	1.059
Final R indexes [I>=2σ (I)]	R_1 = 0.0600, wR_2 = 0.1774
Final R indexes [all data]	R_1 = 0.0663, wR_2 = 0.1890
Largest diff. peak/hole/e·Å^{-3}	0.19/-0.19
Flack parameter	-2.7 (17)

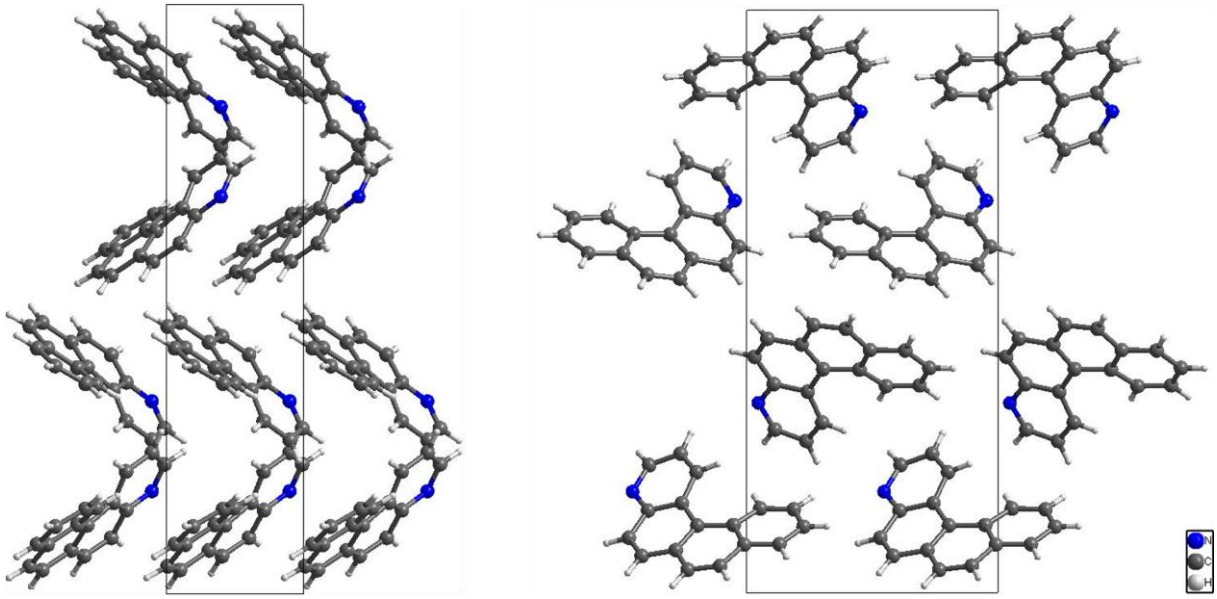

Figure S16. Packing structure of 4-A[4]H in a crystal obtained from a DMF/H_2O (1/99, v/v) mixture.

Table S4. Crystal data and structure refinement for a single crystal of **4-A[4]H** formed in dichloromethane/*n*-pentane

Identification code	4-A[4]H
Empirical formula	$C_{17}H_{11}N$
Formula weight	229.27
Temperature/K	293(2)
Crystal system	orthorhombic
Space group	$Pna2_1$
a/Å	9.6945(17)
b/Å	22.594(7)
c/Å	5.1731(15)
α/°	90
β/°	90
γ/°	90
Volume/Å^3	1133.1(5)
Z	4
$\rho_{Calculated}$ /g·cm^{-3}	1.344
μ/mm^{-1}	0.603
F(000)	480.0
Crystal size/mm^3	0.3 × 0.2 × 0.2
Radiation	CuKα (λ = 1.54178)
2*θ* range for data collection/°	7.826 to 157.57
Index ranges	-12 ≤ h ≤ 12, -28 ≤ k ≤ 28, -5 ≤ l ≤ 6
Reflections collected	17664
Independent reflections	2245 [R_{int} = 0.0557, R_{sigma} = 0.0321]
Data/restraints/parameters	2245/1/163
Goodness-of-fit on F^2	0.896
Final R indexes [I>=2σ (I)]	R_1 = 0.0360, wR_2 = 0.1031
Final R indexes [all data]	R_1 = 0.0405, wR_2 = 0.1088
Largest diff. peak/hole/e·Å^{-3}	0.15/-0.19
Flack parameter	0.0(5)

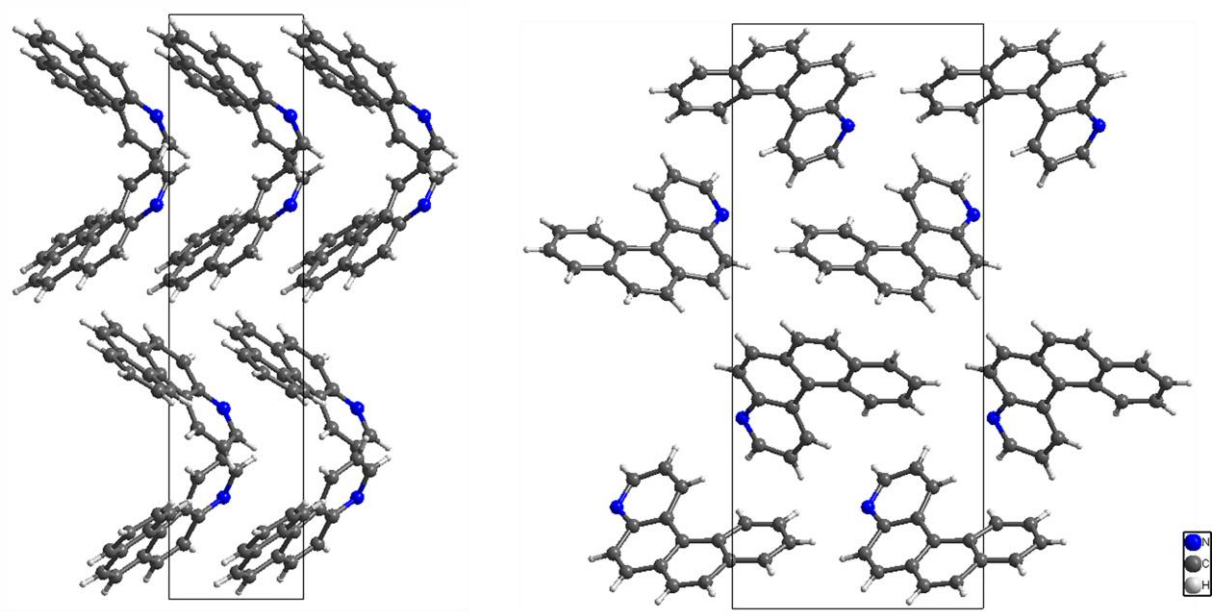

Figure S17. Packing structure of 4-A[4]H in a crystal obtained from a dichloromethane/*n*-pentane mixture by gaseous phase diffusion.

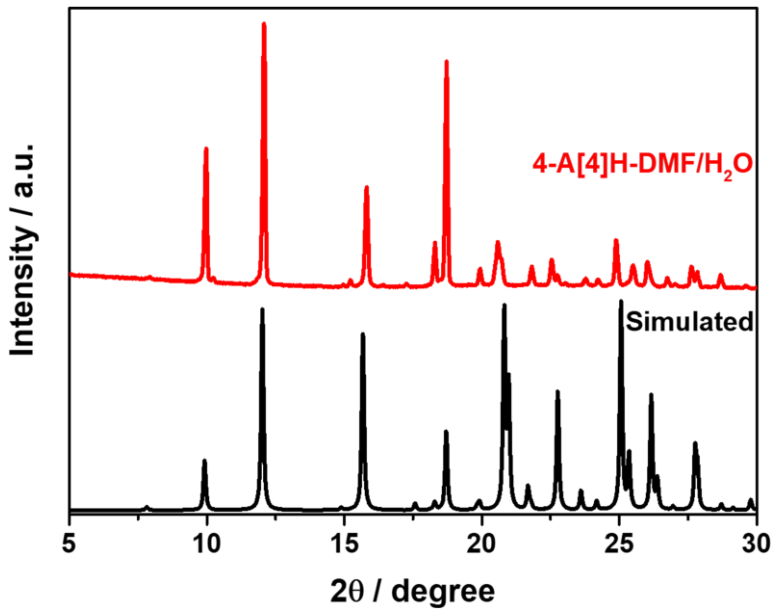

Figure S18. Comparison between simulated powder XRD pattern of a 4-A[4]H crystal formed in a dichloromethane/*n*-pentane mixture and measured powder XRD pattern of 4-A[4]H crystals obtained in DMF/H_2O (1/99, v/v).

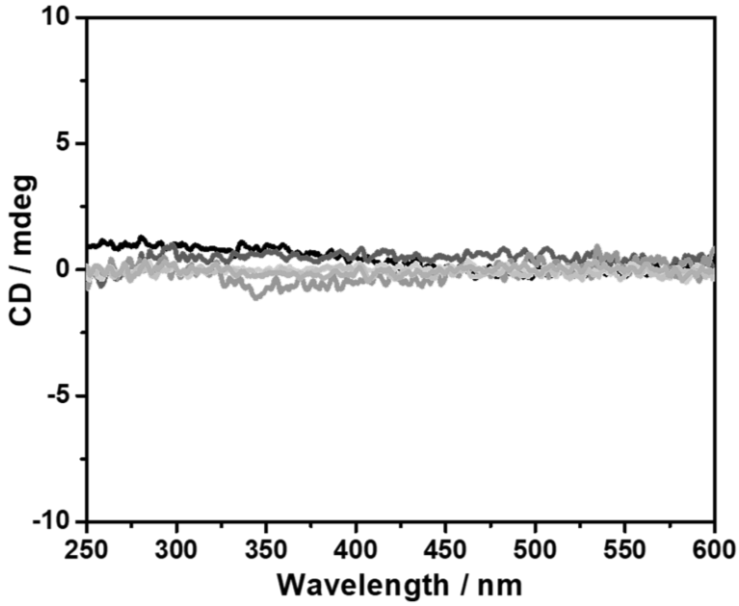

Figure S19. CD spectra of six parallel 2-A[4]H aggregate samples formed in DMF/H_2O (1/99, v/v) with a concentration of 1.3×10^{-3} mol·L^{-1} which were heated to 100 °C in the initial stage.

References

S1. Hewlins, M. J. E.; Salter, R. The photochemical cyclodehydrogenation route to polycyclic azaarenes. *Synthesis* **2007**, *14*, 2164-2174.

S2. (a) Tsuda, A.; Alam, M. A.; Harada, T.; Yamaguchi, T.; Ishii, N.; Aida, T. Spectroscopic visualization of vortex flows using dye-containing nanofibers. *Angew. Chem., Int. Ed.* **2007**, *46*, 8198-8202; (b) Shen, Z.; Jiang, Y.; Wang, T.; Liu, M. Symmetry breaking in the supramolecular gels of an achiral gelator exclusively driven by π-π stacking. *J. Am. Chem. Soc.* **2015**, *137*, 16109-16115; (c) Spitz, C.; Dähne, S.; Ouart, A.; Abraham, H. W. Proof of chirality of J-aggregates spontaneously and enantioselectively generated from achiral dyes. *J. Phys. Chem. B* **2000**, *104*, 8664-8669.